Solvent-Dependent Conformation of the Third Repeat Fragment in the Microtubule-Binding Domain of Tau Protein, Analyzed by ^{1}H-NMR Spectroscopy and Molecular Modeling Calculation

Katsuhiko Minoura,* Koji Tomoo, Toshimasa Ishida, Hiroshi Hasegawa,† Masahiro Sasaki,† and Taizo Taniguchi††

Osaka University of Pharmaceutical Sciences, 4-20-1 Nasahara, Takatsuki, Osaka 569-1094

†Behavioral and Medical Sciences Research Consortium, 2-5-7 Tamachi, Akashi, Hyogo 673-0025

††Biosignal Research Center, Kobe University, 1-1 Rokkodai-cho, Nada, Kobe 657-8501

(Received January 17, 2003)

The third repeat fragment (3MBD, 31 residues) in the four-repeat microtubule-binding domain of tau protein is considered to be responsible for the formation of the neuropathological filament. To clarify the structural function of 3MBD in the filamentous assembly, solution structures in water and 2,2,2-trifluoroethanol (TFE) were investigated by CD measurement and the combination of two-dimensional ^{1}H-NMR measurement and a molecular modeling calculation. The CD spectra suggested the solvent-dependent conformation of 3MBD, i.e., random and α-helical structures in water and TFE solvents, respectively. All protons were assigned by various 2D NMR spectral measurements. The NOE pattern characteristic of a typical helical structure was observed in TFE solution. Using NOE and $J_{HN C\alpha H}$ data observed in both solutions, possible 3D structures were generated by the dynamical simulated annealing method. The constructed NMR conformers in water consisted of an equilibrium mixture of extended and folded conformers, although the N-terminal Val1–Lys6 and middle fragments formed well-refined extended (Val1–Lys6) and α-helical (Leu10–Leu20) structures in TFE, respectively. Interestingly, the helical structure showed an amphipathic distribution of the respective side chains. This amphipathic behaviour of the 3MBD structure is advantageous for self-association through the alternating hydrophilic and hydrophobic interactions into a helical filament of the tau MBD domain. Based on the situation-dependent conformational flexibility of 3MBD, the possibility of filament formation of tau protein via self-assembly of the α-helical structure under neuropathological conditions is discussed.

Microtubules (MTs) are ubiquitous cytoskeletal elements built by the self-association of α,β-tubulin dimers and play an important role in the maintenance of cell shape, cell division, axonal transport, secretion, and receptor activity.[1] Microtubule-associated proteins (MAPs) possess the ability to bind MTs and are believed to play an important role in the regulation of MT formation and stabilization.[2] Tau protein, one of the neuronal MAPs in the mammalian brain, is normally found on axonal MTs and binds to MTs through the MT-binding domain of three or four repeated sequences located in the C-terminal half (Fig. 1).[3,4] The interest in this protein has increased considerably because it is the major component of the pathological lesion characteristic of Alzheimer's disease and other diseases. Also, it has been discovered that the front temporal dementia and Parkinsonism linked to chromosome 17 (FTDP-17), characterized by the formation of neuropathological tau filaments and neuronal cell death, is caused by the mutation of the tau gene encoding the MT-binding domain or close to it.[5–7] In this disease, the mutated tau shows a lower affinity to MTs than the wild one and self-aggregates into a fil-

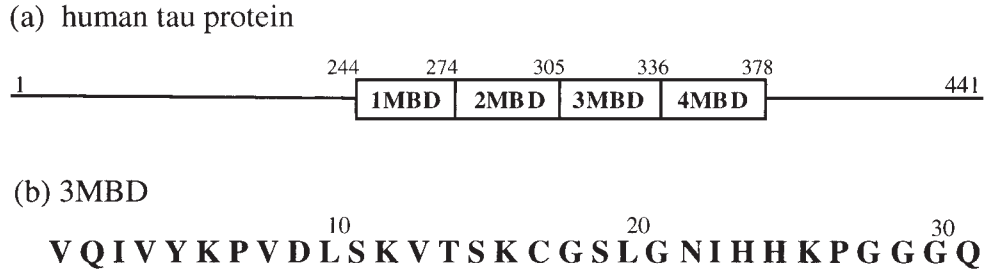

Fig. 1. (a) Schematic diagram of the entire human tau protein including four-repeat MBD. The regions from first to fourth MT-binding repeats are represented by 1MBD to 4MBD, respectively. The numbering of the amino acid residues refers to the longest isoform of human tau (441 residues). (b) Amino acid sequence of 3MBD (the third repeat region 306–336 of tau protein), together with the numbering of amino acid residues used in this work.

Published on the web August 15, 2003; DOI 10.1246/bcsj.76.1617

ament with an aberrant structure.[7,8] Since these aggregates are toxic to neurons, because they obstruct the cell interior, it is important to elucidate the structural features of the tau protein in order to find a possible method for preventing its pathological aggregation.

Regarding the conformation of soluble tau protein in living cells, a definite conclusion has not yet been drawn because of its flexible behavior,[4,9–12] and the structural requisites and mechanism for tau self-assembly are still far from complete understanding. Concerning the self-assembly of tau protein, the following have been confirmed so far. The core of these filaments mainly consists of the three- or four-repeat microtubule-binding domain (MBD),[13] and this domain promotes tau assembly in vitro.[14] Thus, the conformational analysis of MBD should give a clue to elucidating the pathological assembly mechanism of tau protein. Also, it was reported[15] that the VQIVYK sequence in the third repeat of MBD (3MBD, Fig. 1) plays an important role in the assembly of tau protein in Alzheimer paired helical filaments (PHFs).

It's well known that CD spectroscopy is widely used for studying the global conformations of peptides and proteins. In addition, calculation of the molecular dynamics in combination with the conformational constraints (NOEs and coupling constants) obtained from NMR analyses, is a powerful method in determining the stable conformations in solution. In this paper, thus, we report the solvent-dependent 3MBD conformations in water and 2,2,2-trifluoroethanol (TFE) solutions, as studied by CD, ^{1}H-NMR, and molecular modeling methods. Preliminary results obtained using TFE have been reported.[16] An insight into the situation-dependent conformational flexibility of 3MBD is important in understanding the abnormal and insoluble filament aggregation of soluble tau protein.

Experimental

Peptide Syntheses. The 31-residue peptide of 3MBD, corresponding to the third repeat segment 306–336 of human MBD, was purchased from American Peptide Company, Inc. (California, USA). The characterization of 3MBD was performed by mass spectrometry (MALDI-TOF M^+Na = 3270.38 a.m.u. versus the theoretical molecular weight = 3247.8 a.m.u.). The purity was >95.0%, as assessed by reverse-phase HPLC (column: Vydac C-18; eluents: A = H_2O, 0.1% TFA, B = CH_3CN, 0.1% TFA; linear gradient, 10–40% of B; retention time = 13.367 min). The peptide (TFA salt) was obtained as a lyophilized powder.

CD Measurement. The concentration of 3MBD was adjusted to 2.0×10^{-2} mM (1 M = 1 mol dm^{-3}) in water, TFE, and these mixed solvents, where the pH value was adjusted by adding HCl or NaOH. All measurements were conducted at 25 °C with a JASCO J-820 spectrometer in a cuvette with a 2 mm path length. In each experiment, under N_2 gas flow, the measurement from 190 to 260 nm was repeated eight times and the results were summed up. Then, the molar ellipticity was determined after normalizing the peptide concentration. The same experiments were performed at least three times using the newly prepared samples, and their averaged values are given in the paper. Data are expressed in terms of a mean residue ellipticity $[\theta]$ in units of deg cm^2 dmol^{-1}.

NMR Measurements. The sample solution was prepared by dissolving the peptide in H_2O (with 10% D_2O) or TFE-d_2. The ^{1}H-NMR spectra were recorded on a Varian unity INOVA500 spectrometer with a variable temperature-control unit. The proton chemical shifts were referenced to 0 ppm for 3-(trimethylsilyl)propionic acid (TSP). From NMR measurements at different pHs and temperatures, the most suitable conditions for conventional NMR measurements were determined to be as follows: peptide concentration = 2 mM, temperature = 298 K, and pH = 4.2 (H_2O) and 3.9 (TFE-d_2). The solution of pH > 5.0 led to decreased solubility of the peptide. The pH value was adjusted by adding HCl or NaOH. For the concentration-dependence experiment, the chemical shift of each NH proton was measured under three different concentrations (0.5 mM, 1.0 mM and 2.0 mM) because of the solubility problem. For the temperature-dependence experiment, the chemical shift of each NH proton was measured in the range of 20 °C to 60 °C (10 °C intervals).

The 2D DQF-COSY, TOCSY and NOESY spectra were acquired in the phase-sensitive mode using standard pulse programs available in the Varian software library. Continuous low-power irradiation was performed during the relaxation delay to suppress the peak due to water. Spectra were zero-filled to achieve a digital resolution of 1.3 Hz/point. In order to follow direct single- and multiple-relayed through-bond connectivities, TOCSY spectra were recorded at mixing times of 70 and 120 ms. NOESY spectra were also measured at mixing times of 200 ms to 500 ms (100 ms intervals) for H_2O and 100 ms, 200 ms and 300 ms for TFE-d_2. The NOE intensities were classified into three groups (strong, medium, and weak).

In addition, the vicinal coupling constants by DQF-COSY measurements were used to estimate possible ϕ torsion angles: $^3J_{HNC\alpha H} = 1.9 - 1.4\cos\theta + 6.4\cos^2\theta$, where $\theta = |\phi - 60|^\circ$ for ϕ torsion angle around the C'_{i-1}–N_i–$C\alpha_i$–C'_i bond sequence.[17]

Computational Molecular Modeling Based on Proton-Proton Distance and ϕ Torsion Angle Constraints. Various 3D structures that satisfy the NOE and torsion angle constraints of intramolecular proton pairs were constructed by dynamical SA (simulated annealing) calculations[18,19] operating on the CNS[20] program. After the randomization of the peptide into the extended strand corresponding to each disjointed molecular entity, the pro-

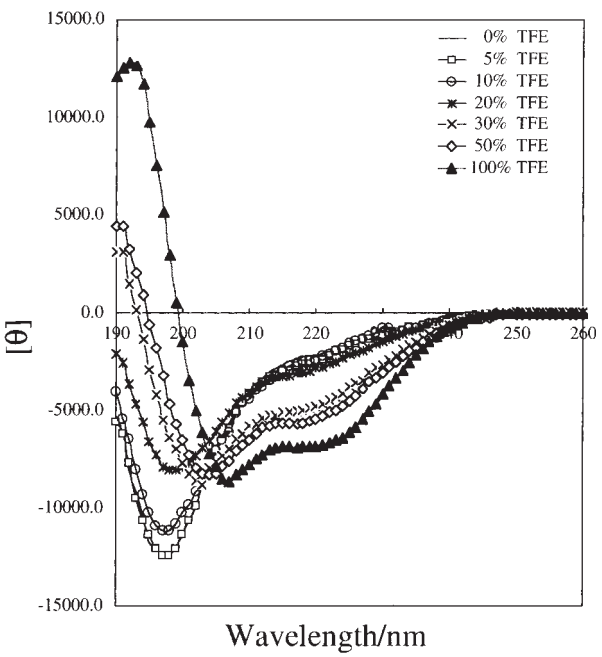

Fig. 2. CD spectra of 3MBD at different ratios of water/TFE mixtures at pH 7.0.

tocol for the SA calculation consisted of reading the various structural parameters and of the initialization for statistical analysis of the average property. The torsion angles were then annealed for 15 ps at 50000 K and cooled to 300 K with a slope of 250 K/step over 10 ps. After that, the minimization of the peptide was continued for 5000 steps. The constraints for distances and torsion angles were modeled as harmonic potential functions. As input data for the distance constraint, the proton-proton pairs were classified into three groups according to NOE intensities: strong (1.8–3.0 Å), medium (1.8–4.0 Å) and weak (1.8–5.0 Å). For ϕ torsion angle constraints, the following were applied: $-120 \pm 40^\circ$ for $^3J_{HN\alpha H} > 8$ Hz, $-110 \pm 50^\circ$ for $^3J_{HN\alpha H} > 7$ Hz, $-75 \pm 25^\circ$ for $^3J_{HN\alpha H} < 6$ Hz, and $-100 \pm 60^\circ$ for the others. RMSD analyses of the energy-minimized structures were carried out with the program MOLMOL.[21]

Results

CD Spectroscopy. To estimate the solvent-dependent flexibility of the 3MBD conformation, the CD spectra were measured at different ratios of a water/TFE mixture (pHs 4.2 and 7.0), and the results obtained at pH 7.0 are shown in Fig. 2. Nearly the same profile was observed at pH 4.2. Although the quantification of CD spectra in terms of secondary structure components is often unreliable, the general shapes of the spectra are significantly accurate because they reveal gross conformational states. The spectrum of 3MBD in water is indicative of a predominantly random conformation characterized by a negative peak around 197 nm, together with little effect on the peptide conformation of the pH variation. In contrast, the CD spectra in TFE indicate an α-helical structure characterized by two negative peaks around 209 nm and 222 nm, the conformation of which is reversibly transformed to a random structure by adding water to the TFE solution. The conformational intermediate is formed at 10% to 20% TFE aqueous solution, and is little affected by the pH change. Such conformational change is fast and has no time dependence. These results indicate that the helical conformation of 3MBD is flexible enough to change into a random structure depending on the hydrophobic/hydrophilic balance of the solvent, and is insensitive to the pH change.

Resonance Assignment. Proton peak assignments for 3MBD were performed by a combination of (a) the connectivity information via scalar coupling in phase-sensitive TOCSY experiments and (b) the sequential NOE networks along the peptide backbone protons. Although peak assignment in H_2O was performed for most protons, those of Asp9, Asn22, His24 and His25 were confirmed by the measurement in D_2O solution because of the extensive overlapping with water protons. The longer mixing time of 120 ms made complete observation of the Lys side chain possible. Similarly, the peak assignment in TFE solution was performed for most protons, except for those of Lys16, Ser19, Pro27 and Gln31. The peak

Table 1. ^{1}H NMR Chemical Shifts (in ppm) of 3MBD at 298 K in Water/D_2O (9:1 v/v) and pH = 4.2[a)]

	Assignment	Chemical shifts[a)] of			
		NH	CαH	CβH	Others
1	Val		3.821	2.198	1.000, 1.006
2	Gln	8.706	4.439	1.985, 2.270	2.324
3	Ile	8.432	4.102	1.748	0.710, 0.830, 1.142, 1.443
4	Val	8.219	4.084	1.958	0.864, 0.894
5	Tyr	8.446	4.560	2.938	6.792, 7.110
6	Lys	8.177	4.555	1.643	1.387, 1.728, 2.967
7	Pro		4.364	1.904, 2.289	2.003, 3.598
8	Val	8.183	4.020	2.030	0.919, 0.963
9	Asp	8.388	4.668	2.806, 2.631	
10	Leu	8.504	4.319	1.660	0.850, 0.936, 1.660
11	Ser	8.423	4.328	3.917	
12	Lys	8.008	4.383	1.760, 1.900	1.380, 1.450, 1.659, 2.983
13	Val	7.921	4.166	2.124	0.943, 0.967
14	Thr	8.237	4.396	4.245	1.213
15	Ser	8.281	4.470	3.869	
16	Lys	8.436	4.376	1.683	1.443, 1.780, 1.879, 3.003
17	Cys	8.359	4.509	2.949	
18	Gly	8.481	3.994, 4.024		
19	Ser	8.248	4.470	3.869	
20	Leu	8.353	4.358	1.620	0.871, 0.926, 1.680
21	Gly	8.331	3.923		
22	Asn	8.277	4.705	2.731, 2.817	
23	Ile	7.964	4.074	1.798	0.740, 0.798, 1.106, 1.231
24	His	8.555	4.728	3.130, 3.229	7.275, 8.599
25	His	8.455	4.689	3.146, 3.235	7.283, 8.612
26	Lys	8.560	4.594	1.687	1.460, 1.809, 3.003
27	Pro		4.440	1.976, 2.330	2.030, 2.088, 3.670, 3.868
28	Gly	8.612	3.935, 4.075		
29	Gly	8.341	3.961		
30	Gly	8.315	4.007		
31	Gln	7.964	4.195	1.932, 2.124	2.298

a) ^{1}H chemical shifts were referenced to 0 ppm for TSP.

Table 2. ^{1}H NMR Chemical Shifts (in ppm) of 3MBD at 298 K in TFE and pH = 3.9[a)]

	Assignment	Chemical shifts[a)] of			
		NH	CαH	CβH	Others
1	Val		3.608	2.186	1.041, 1.062
2	Gln	n.d.	4.438	2.052, 2.146	2.429, 6.176, 7.046
3	Ile	7.435	4.181	1.910	0.919, 0.930, 1.228, 1.509
4	Val	7.209	4.052	2.042	0.873, 0.899
5	Tyr	7.388	4.614	2.956, 3.099	6.826, 7.107
6	Lys	7.841	4.664	1.836	1.558, 1.855, 1.889, 3.059
7	Pro		4.408	2.337	2.052, 2.180, 3.668, 3.744
8	Val	7.247	3.958	2.156	1.006, 1.056
9	Asp	7.766	4.669	2.874	
10	Leu	7.982	4.198	1.802	0.940, 0.996, 1.733
11	Ser	8.382	4.312	4.108	
12	Lys	7.778	4.120	2.163	1.540, 1.782, 1.992, 3.054
13	Val	7.951	3.840	2.219	1.042, 1.123
14	Thr	8.360	4.027	4.313	1.360
15	Ser	7.930	4.295	4.124	
16	Lys	7.947	4.237	2.101	1.548, 1.610, 1.788, 3.033
17	Cys	8.446	4.236	2.959, 3.102	
18	Gly	8.623	3.972, 4.004		
19	Ser	7.940	4.394	4.065, 4.146	
20	Leu	7.907	4.281	1.944	0.952, 1.007, 1.647
21	Gly	8.160	3.975		
22	Asn	7.940	4.655	2.936	
23	Ile	7.796	4.035	1.966	0.853, 0.896, 1.265, 1.484
24	His	7.874	4.630	3.178, 3.354	7.247, 8.236
25	His	7.928	4.791	3.266, 3.432	7.282, 8.363
26	Lys	8.028	4.722	1.755	1.503, 1.888, 3.063
27	Pro		4.343	2.380	2.015, 2.221, 3.651, 3.854
28	Gly	7.952	3.742, 4.248		
29	Gly	8.130	3.934, 4.118		
30	Gly	7.771	3.978, 4.026		
31	Gln	7.488	4.336	2.010, 2.216	2.374, 6.242, 7.069

a) ^{1}H chemical shifts were referenced to 0 ppm for TSP.

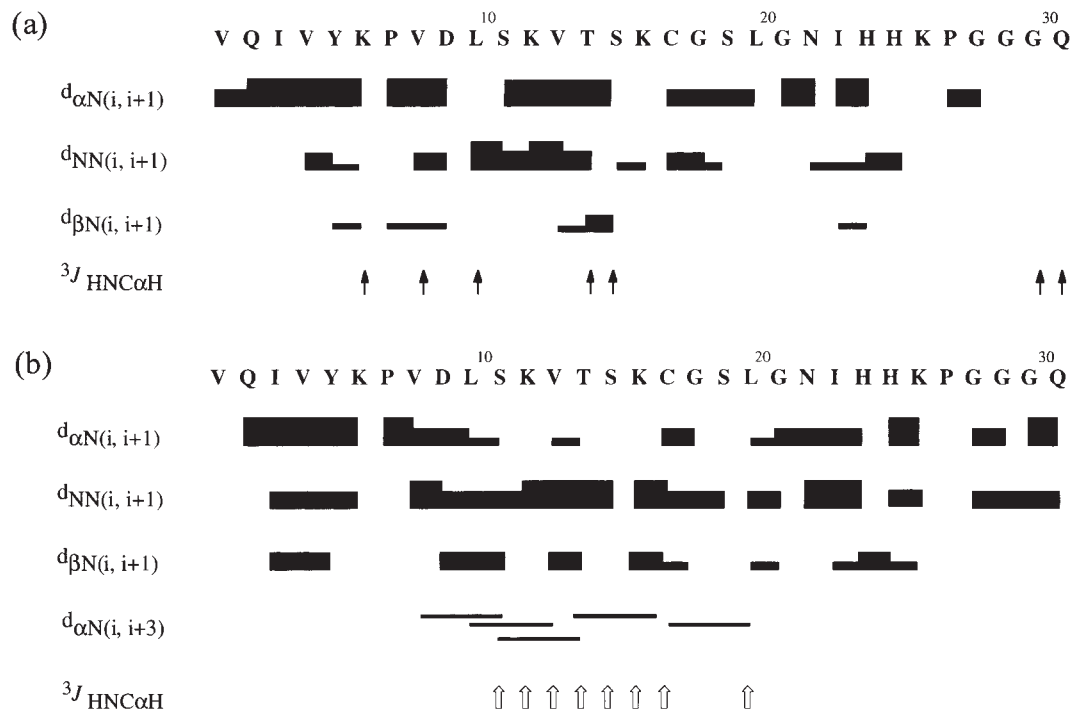

Fig. 3. Diagram of NOE connectivities between neighboring ($d_{\alpha N(i,i+1)}$, $d_{NN(i,i+1)}$, $d_{\beta N(i,i+1)}$, and $d_{\alpha N(i,i+3)}$) protons and *j*-coupling constants ($^3J_{HN C\alpha H}$). (⇑) Coupling constant > 8 Hz; (⇧) coupling constant < 6 Hz observed in H_2O (a) and TFE (b). The strength of the observed NOE is represented by the thickness of the bars.

Table 3. Temperature and Concentration Coefficients of NH Protons

Residue	H_2O		TFE	
	$\Delta\delta/\Delta T$ (ppb/K)	$\Delta\delta/\Delta C$ (ppb/mM)	$\Delta\delta/\Delta T$ (ppb/K)	$\Delta\delta/\Delta C$ (ppb/mM)
Val1				
Gln2	−6.0	1.7		
Ile3	−8.3	2.0	−3.3	1.1
Val4	−7.7	0.0	−2.2	0.0
Tyr5	−9.0	0.7	−2.5	0.2
Lys6	−6.5	−2.0	−3.2	0.3
Pro7				
Val8	−8.0	1.7	−2.5	0.5
Asp9	−7.3	1.7	−1.5	0.3
Leu10	−9.4	−6.0	−3.2	0.0
Ser11	−4.7	−5.3	−1.7	0.0
Lys12	−4.6	2.0	−1.1	0.2
Val13	−5.1	6.0	−1.8	−0.3
Thr14	−7.1	2.7	−1.7	0.1
Ser15	−7.2	−6.0	−1.5	−0.2
Lys16	−7.7	0.0	−1.6	0.0
Cys17	−6.3	0.7	−1.3	0.0
Gly18	−6.4	−2.0	−1.6	0.4
Ser19	−5.7	2.0	−1.7	0.2
Leu20	−7.2	0.0	−1.2	0.0
Gly21	−5.8	0.7	−2.4	0.3
Asn22	−5.0	−2.0	−2.2	−0.3
Ile23	−6.2	2.7	−2.5	0.6
His24	−7.0	2.0	−2.1	0.8
His25	−6.6	1.7	−0.7	0.2
Lys26	−7.6	1.7	−2.3	0.5
Pro27				
Gly28	−7.8	−1.7	−3.8	1.3
Gly29	−5.8	2.7	−2.5	0.8
Gly30	−5.4	2.0	−2.9	−0.8
Gln31	−6.4	4.0	−2.1	1.5

assignments of these two pairs of residues (Lys16/Ser19 and Pro27/Gln31) were confirmed by measurement in solution at different temperatures because of peak overlap. The Gln2 NH proton was not detected. The chemical shifts of respective protons in H_2O and TFE solutions are summarized in Tables 1 and 2, respectively.

Amide NH Protons. The situation of NH groups in solution could be estimated by measuring the temperature and concentration dependence of their chemical shifts. The chemical shifts of exposed protons are strongly influenced by any environmental change. The changes of NH chemical shifts were thus measured as a function of temperature and concentration, and are given in Table 3. In H_2O solution, the large temperature slope ($\Delta\delta/\Delta T$) was spread over a relatively wide range of −4.6 to −9.4 ppb/K, indicating a flexible, random conformation, where the NH protons are exposed to water molecules. This is also suggested by the fast H–D exchange (<5 min) of all amide protons. In contrast, all NH protons in TFE solution showed a small $\Delta\delta/\Delta T$ slope of −0.7 to −3.8 ppb/K, indicating the shielding of NH protons from the solvent in any secondary structure. In particular, the successive low temperature coefficients of NH protons ($\Delta\delta/\Delta T = -1.8$ to -1.1 ppb/K) on the Ser11–Leu20 sequence indicate their participation in intramolecular hydrogen bond formation. On the other hand, the lack of a significant concentration dependence of $\Delta\delta/\Delta C$ (0.5 ± 2.8 ppb/mM for H_2O, 0.3 ± 0.5 ppb/mM for TFE, on average) suggests a small population of the molecules in the associated state. To further check the possibility of molecular association, 1D spectra of 3MBD in both solutions were compared at 0.5 mM and 2 mM concentrations under the otherwise same conditions. In the high-field region, the spectra were completely congruent, and no protons larger than $\Delta\delta = \pm 0.01$ ppm were observed in the exchangeable region. The NH-Hα coupling constants were not changed at either concentration. These results also suggest a small population in the associated state under this NMR condition.

Table 4. Structural Statistics for 20 Stable Structures of 3MBD Domain

Solvent	H_2O	TFE
Number of constraints:		
Total number of NOEs	181	273
Intra-residue NOEs	114	157
Sequential NOEs	55	82
Inter-residue NOEs	2	34
Dihedral angles	23	23
	Average values (esd)	
RMS deviation (N, Cα C′)	1.0(3)[a]	0.6(2)[b]
RMS deviation from NOE (Å)	0.008(1)	0.008(1)
NOE violations > 0.10 Å	0.1(1)	3.2(4)
Energy (kJ/mol)		
overall	69.0(7)	353(9)
noe	3.4(1)	135(5)
angle	60.1(2)	127(5)
bond	0.7(1)	30(1)
improper	1.1(1)	27(1)
van der Waals	3.7(5)	34(5)

a) Calculated from residues 10 to 15. b) Calculated from residues 10 to 20.

Proton-Proton Distance. NOESY spectra were measured to observe short-, medium- and long-range proton-proton connectivity along the peptide backbone. The results are summarized in Fig. 3 and Table 4. Strong NOEs of CαH (Lys6)–CδH (Pro7) and CαH (Lys26)–CδH (Pro27) proton pairs suggest the *trans* orientation around the Lys6–Pro7 and Lys26–Pro27 ωbonds in both solutions. Compared with typical NOESY cross-peaks among neighbouring protons for the helical, sheet, or turn structures of a polypeptide,[22] the pattern of 3MBD in H_2O showed no existence of such a secondary structure. In contrast, the NOE connectivities between $d_{\alpha N(i,i-1)}$ and $d_{NN(i,i+1)}$ in the 2–6 sequence and between $d_{NN(i,i+1)}$ and $d_{\alpha N(i,i+3)}$ in the 10–20 sequence in TFE solution (Fig. 3) suggested extended and α-helix structures of these sequences, respectively. By using 181 (H_2O) and 273 (TFE-d_2) NOE constraints for proton-proton distances and 23 $^3J_{HN C\alpha H}$ constraints for ϕ torsion angles, the possible major conformers were then constructed by the following molecular modeling calculations.

Molecular Modeling by Dynamical SA Calculations. One hundred 3D structures of 3MBD were constructed by the dynamical SA method imposing the distance and torsion angle constraints. The statistics for the constructed 3D struc-

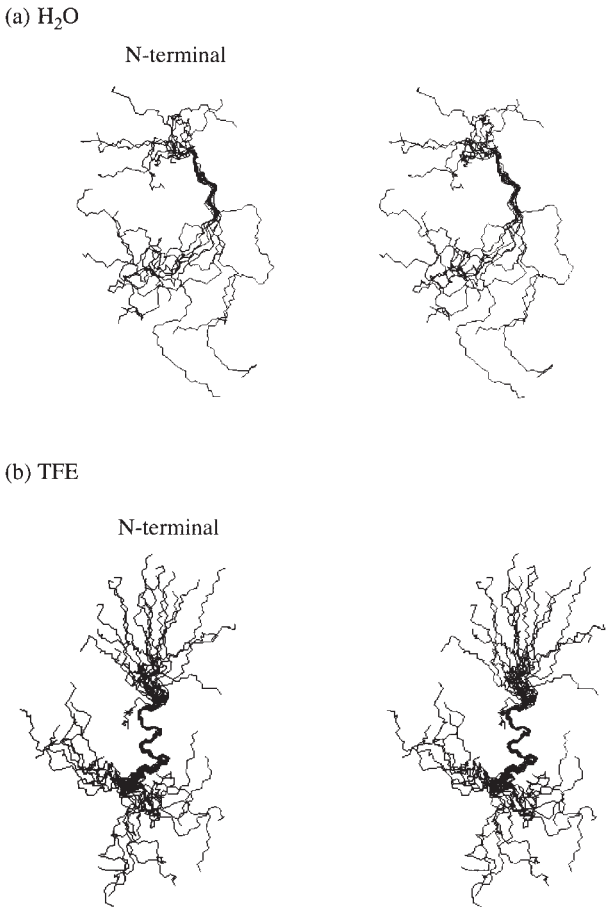

Fig. 4. Stereoscopic superposition of 3MBD in each solution. (a) The 10 most stable conformers projected in order to superimpose the Leu10–Ser15 sequence. (b) The 20 most stable conformers projected in order to superimpose the Leu10–Leu20 sequence.

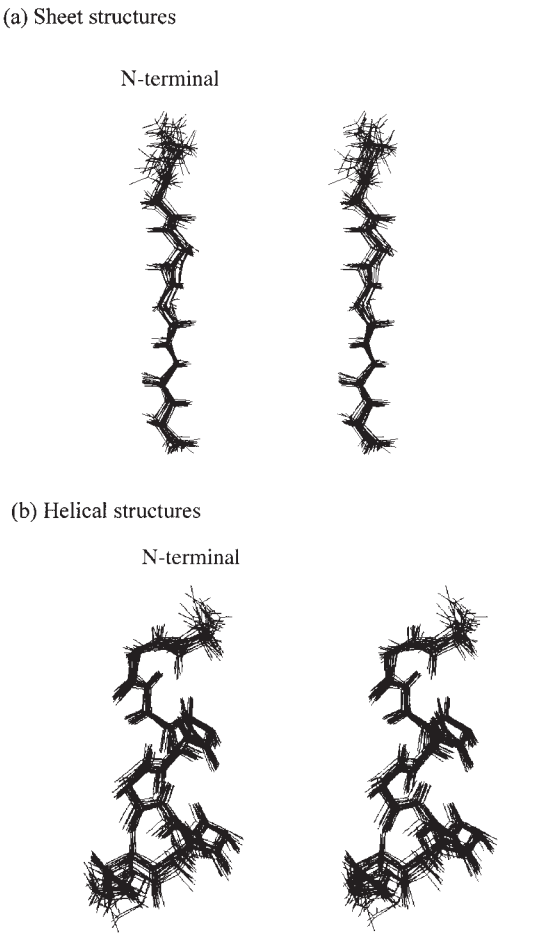

Fig. 5. Stereoscopic superposition of the 20 most stable partial 3MBD conformers in TFE solution: (a) sheet structures of Val1–Lys6 sequences and (b) helical structures of Leu10–Leu20 sequence.

tures are summarized in Table 4, and the superpositions of the most stable 20 conformers in respective solutions are shown in Fig. 4. In H_2O solution, none of the peptides produced well-refined conformers that agreed perfectly with all constraints imposed in the model. This may have resulted from the insufficient NOEs for rigorous structural determination, in addition to the widely defined limitations for proton-proton distances. The respective conformers roughly converged into two each of extended and folded forms based on their backbone conformation. On a whole, therefore, it could be said that 3MBD in H_2O consists of an equilibrium mixture of many extended and folded conformers. On the other hand, the N-terminal Val1–Lys6 and middle Leu10–Leu20 fragments of 3MBD in TFE were well refined by the NMR data constraints for defining the extended and α-helical structures, respectively (Fig. 5), whereas the loops connecting these two secondary structures and the C-terminal moiety were not rigid enough to make any 3D structure, thus leading to both open and folded forms as the overall structure (Fig. 4).

Discussion

Regarding the overall conformation of soluble tau protein, its detailed structure is unknown at present, and the understanding of the structural requisites and mechanism for tau self-assembly is still far from complete. In such a situation, the conformational study of the 3MBD fragment is important when considering the self-aggregation mechanism of tau protein (Fig. 1), because this fragment is believed to constitute the core moiety for toxic filament formation.[15,23,24] Thus, this work was performed to clarify whether 3MBD has any core structural elements for filament formation.

The CD spectra (Fig. 2) showed the reversible and fast exchange between the random structure in H_2O and the α-helical one in TFE, where the intermediate state is formed at a 10–20% TFE/H_2O mixture and is little affected by pH change. From this observation, it could be said that this peptide is flexible enough to change its structure depending on the hydrophilic/hydrophobic balance of the solvent.

In order to estimate the flexibility or rigidity of the conformation of 3MBD in H_2O and TFE solvents, possible solution conformations were determined by a combination of ^{1}H NMR spectroscopic and molecular dynamical SA methods. The results showed that 3MBD in H_2O is an equilibrium mixture of many extended and folded conformers, although the relatively less flexible moiety was observed for the extended structures of the N-terminal VQIVYK and the middle Leu10–Ser15

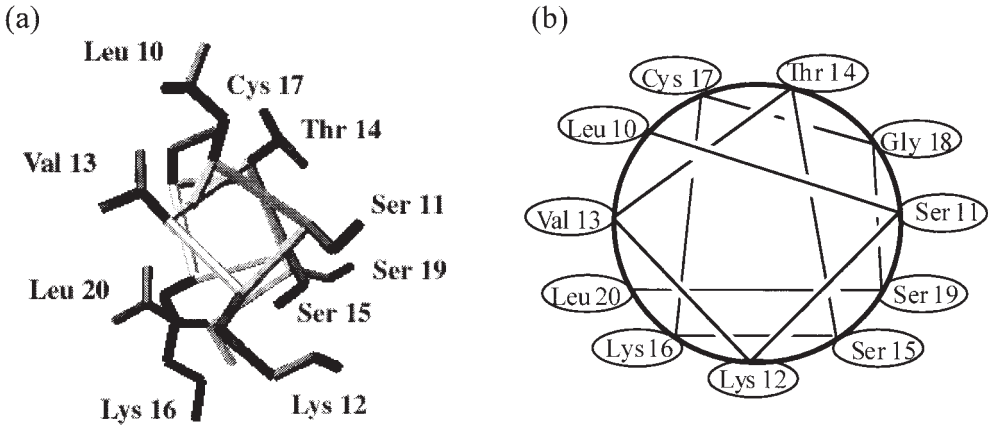

Fig. 6. Helical wheel drawing (a) and schematic diagram (b) of the Leu10–Leu20 sequence of the most stable conformer of 3MBD in TFE, viewed down from the N-terminal side.

sequences. In contrast, 3MBD in TFE showed the extended structure of the N-terminal VQIVYK and the α-helical one of the middle Leu10–Leu20 sequence with clear NOE peak connectivity, whereas the loop region connecting these secondary structures and the C-terminal moiety were flexible and did not make any definite 3D structure.

The VQIVYK sequence in 3MBD is known to be necessary for the assembly of tau protein into Alzheimer PHFs,[15] and thus the extended structure of this sequence observed in both H_2O and TFE solvents may be important as a trigger for self-aggregation. On the other hand, the sequence of Leu10–Leu20 formed a well-defined α-helical structure only in TFE: the RMS deviation of the backbone is 0.55 Å. Interestingly, the helix wheel drawing of this sequence shows an amphipathic distribution of the respective amino acid residues (Fig. 6). The hydrophobic residues of Leu10 and Val13 and the hydrophilic residues of Ser11, Thr14, Ser15, and Ser19 are arranged on the two sides of the helix axis, respectively, and the polar residues of Cys17, Lys12, and Lys16 are located at the interface between the two sides. Although the biological function of such a helical orientation of 3MBD in TFE solution is not clear at the present, it is worth noting that some model peptides having the amphiphilic α-helical nature show a structural transition to β-fibril under appropriate hydrophobic conditions.[25–30] Together with the CD spectra showing the helical conformations of 2MBD and 4MBD (Fig. 1) in TFE solution (data are not shown), the following consideration is possible for the self-assembly of tau protein. An assembly model of MBD is shown in Fig. 7, which proposes the dimer formation of the monomeric helical structure due to hydrophobic interactions and the molecular aggregation of these dimer structures due to hydrophilic interaction. In this model, the piling axis of the assembly is at right angles to each MBD molecule; a similar model has already been proposed by Friedhoff et al.[13] As the assembly proceeds, the structure of the α-helix aggregates transforms into a β-sheet structure in a hydrophilic environment, such as that of a living cell, because of the thermodynamic advantage of the latter structure compared with the former one. The extended structure of the N-terminal VQIVYK of 3MBD may be an important trigger for the transformation of tau protein to the β-sheet structure.

In conclusion, the present results revealed that 3MBD is highly flexible, and the transition between the extended and folded conformers is easily performed depending on the hydrophilic/hydrophobic balance of the surrounding solvent. The amphipathic helical structure of 3MBD in TFE, shown for the first time in the present work, led to the proposal of an MBD-nucleated assembly model of tau protein. This proposal

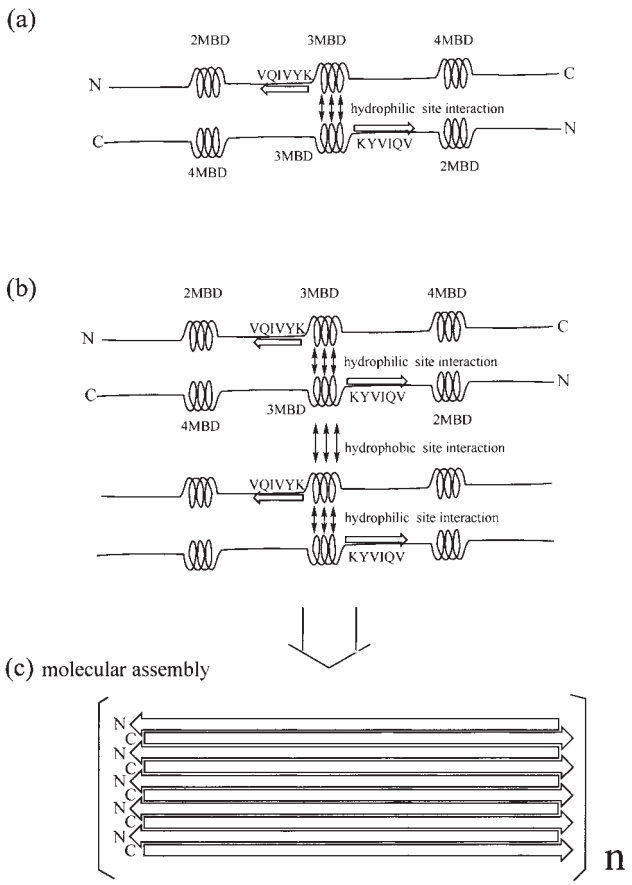

Fig. 7. Assembly model of MBD. Self-assembly is performed via (a) the dimer formation of the monomeric helical structure due to the hydrophobic interaction and (b) the molecular aggregation of these dimer structures due to the hydrophilic interaction.

may be useful for understanding the biological events occurring at the initial step of abnormal filament aggregation of tau protein in Alzheimer's disease.

This work was supported by Grants-in-Aid for Scientific Research from the Ministry of Education, Culture, Sports, Science and Technology of Japan and by The Science Research Promotion Fund of The Promotion and Mutual Aid Corporation for Private Schools of Japan.

References

1 R. D. Burgoyne, "The Neuronal Cytoskeleton", Wiley-Liss, Inc., New York (1991).

2 M. Goedert, R. Jakes, M. G. Spillantini, and R. A. Crowther, in "Microtubules", ed by J. Hyams and C. Lloyd, Wiley-Liss, Inc., New York (1994), p. 183.

3 L. Varani, M. Hasegawa, M. G. Spillantini, M. J. Smith, J. R. Murrell, B. Ghetti, A. Klug, M. Goedert, and G. Varani, *Proc. Natl. Acad. Sci. U.S.A.*, **96**, 8229 (1999).

4 P. Friedhoff, M. von Bergen, E. M. Mandelkow, and E. Mandelkow, *Biochim. Biophys. Acta*, **1502**, 122 (2000).

5 M. Goedert, A. Crowther, and M. G. Spillantini, *Neuron*, **21**, 955 (1998).

6 M. G. Spillantini, T. D. Bird, and B. Ghetti, *Brain Pathol.*, **8**, 387 (1998).

7 M. Goedert and M. G. Spillantini, *Biochim. Biophys. Acta*, **1502**, 110 (2000).

8 M. Hasegawa, M. J. Smith, and M. Goedert, *FEBS Lett.*, **437**, 207 (1998).

9 O. Schweers, E. Schonbrunn-Hanebeck, A. Marx, and E. Mandelkow, *J. Biol. Chem.*, **269**, 24290 (1994).

10 M. Goedert, R. Jakes, and R. A. Crowther, *FEBS. Lett.*, **450**, 306 (1999).

11 D. W. Cleveland, S. Y. Hwo, and M. W. Kirschner, *J. Mol. Biol.*, **116**, 227 (1997).

12 G. A. Jicha, J. M. Rockwood, B. Berenfeld, M. Hutton, and P. Davies, *Neurosci. Lett.*, **260**, 153 (1999).

13 P. Friedhoff, M. von Bergen, E. M. Mandelkow, and E. Mandelkow, *Proc. Natl. Acad. Sci. U.S.A.*, **95**, 15712 (1998).

14 H. Wille, G. Drewes, J. Biernat, E. M. Mandelkow, and E. Mandelkow, *J. Cell Biol.*, **118**, 573 (1992).

15 M. von Bergen, P. Friedhoff, J. Biernat, J. Heberle, E. M. Mandelkow, and E. Mandelkow, *Proc. Natl. Acad. Sci. U.S.A.*, **97**, 5129 (2000).

16 K. Minoura, K. Tomoo, T. Ishida, H. Hasegawa, M. Sasaki, and T. Taniguchi, *Biochem. Biophys. Res. Commun.*, **294**, 210 (2002).

17 V. F. Bystrov, *Prog. Nucl. Magn. Reson. Spectrosc.*, **10**, 41 (1976).

18 G. M. Clore, M. Nigles, D. K. Sukumaran, A. T. Bruenger, M. Karplus, and A. M. Gronenborn, *EMBO J.*, **5**, 2729 (1986).

19 M. Nilges, G. M. Clore, and A. M. Gronenborn, *FEBS Lett.*, **229**, 317 (1988).

20 A. T. Brunger, P. D. Adams, G. M. Clore, W. L. DeLano, P. Gros, and R. W. Grosse-Kunstleve, *Acta Crystallogr., Sect. D*, **54**, 905 (1998).

21 R. Koradi, M. Billeter, and K. Wuthrich, *J. Mol. Graphics*, **14**, 51 (1996).

22 G. Wagner, D. Neuhaus, E. Worgotter, M. Vasak, J. R. H. Kagi, and K. Wuthrich, *J. Mol. Biol.*, **187**, 131 (1986).

23 B. L. Goode, M. Chau, P. E. Denis, and S. C. Feinstein, *J. Biol. Chem.*, **275**, 38182 (2000).

24 R. Hoffmann, N. Dawson, J. D. Wade, and J. Jr. Otvos, *J. Peptide Sci.*, **50**, 132 (1997).

25 M. Mutter and R. Hersperger, *Angew. Chem., Int. Ed. Engl.*, **29**, 185 (1990).

26 J. Nguyen, M. A. Baldwin, F. E. Cohen, and S. B. Prusiner, *Biochemistry*, **34**, 4186 (1995).

27 S. Ono, N. Kameda, T. Yoshimura, C. Shimasaki, E. Tsukuromichi, H. Mihara, and N. Nishino, *Chem. Lett.*, **1995**, 965.

28 H. Mihara and Y. Takahashi, *Curr. Opin. Struct. Biol.*, **7**, 501 (1997).

29 F. Chiti, P. Webster, N. Taddei, A. Clark, M. Stefani, G. Ramponi, and C. M. Dobson, *Proc. Natl. Acad. Sci. U.S.A.*, **96**, 3590 (1999).

30 Y. Takahashi, A. Ueno, and H. Mihara, *Bioorg. Med. Chem.*, **7**, 177 (1999).